PHYSICAL REVIEW B **83**, 220515(R) (2011)

Antiferromagnetic spin excitations in single crystals of nonsuperconducting $Li_{1-x}FeAs$

Meng Wang,[1,2] X. C. Wang,[1] D. L. Abernathy,[3] L. W. Harriger,[2] H. Q. Luo,[1] Yang Zhao,[4,5] J. W. Lynn,[4] Q. Q. Liu,[1] C. Q. Jin,[1] Chen Fang,[6] Jiangping Hu,[6,1] and Pengcheng Dai[2,3,1,*]

[1]*Beijing National Laboratory for Condensed Matter Physics, Institute of Physics, Chinese Academy of Sciences, Beijing 100190, China*

[2]*Department of Physics and Astronomy, The University of Tennessee, Knoxville, Tennessee 37996-1200, USA*

[3]*Neutron Scattering Science Division, Oak Ridge National Laboratory, Oak Ridge, Tennessee 37831-6393, USA*

[4]*NIST Center for Neutron Research, National Institute of Standards and Technology, Gaithersburg, Maryland 20899, USA*

[5]*Department of Materials Science and Engineering, University of Maryland, College Park, Maryland 20742, USA*

[6]*Department of Physics, Purdue University, West Lafayette, Indiana 47907, USA*

(Received 18 April 2011; revised manuscript received 27 May 2011; published 24 June 2011)

We use neutron scattering to determine spin excitations in single crystals of nonsuperconducting $Li_{1-x}FeAs$ throughout the Brillouin zone. Although angle resolved photoemission experiments and local density approximation calculations suggest poor Fermi surface nesting conditions for antiferromagnetic (AF) order, spin excitations in $Li_{1-x}FeAs$ occur at the AF wave vectors $Q = (1,0)$ at low energies, but move to wave vectors $Q = (\pm 0.5, \pm 0.5)$ near the zone boundary with a total magnetic bandwidth comparable to that of $BaFe_2As_2$. These results reveal that AF spin excitations still dominate the low-energy physics of these materials and suggest both itinerancy and strong electron-electron correlations are essential to understand the measured magnetic excitations.

DOI: 10.1103/PhysRevB.83.220515 PACS number(s): 74.70.Xa, 74.25.Ha, 78.70.Nx

Understanding whether magnetism is responsible for superconductivity in FeAs-based materials continues to be one of the most important unresolved problems in modern condensed matter physics.[1–3] For a typical iron arsenide such as LaFeAsO,[4] band structure calculations predict the presence of the hole-like Fermi surfaces at the $\Gamma(0,0)$ point and electron-like Fermi surfaces at the $M(1,0)/(0,1)$ points in the Brillouin zone [Fig. 1(a)].[5] As a consequence, Fermi surface nesting and quasiparticle excitations between the hole and electron pockets can give rise to static antiferromagnetic (AF) spin-density-wave order at the in-plane wave vector $Q = (1,0)$.[6] Indeed, neutron scattering experiments have shown the presence of the $Q = (1,0)$ AF order in the parent compounds of iron arsenide superconductors, and doping to induce superconductivity suppresses the static AF order.[7] In addition, angle-resolved photoemission measurements[8] have confirmed the expected hole and electron pockets in superconducting iron arsenides, thus providing evidence for superconductivity arising from the sign revised electron-hole interpocket quasiparticle excitations.[5,9–12]

Of all the FeAs-based superconductors,[1] LiFeAs is special since it has the highest transition temperature ($T_c = 18$ K) amongst the stoichiometric compounds.[13–17] Furthermore, it does not have static AF order due to the poor Fermi surface nesting properties with shallow hole pockets near the $\Gamma(0,0)$.[18] It has been suggested that the flat tops of the hole pockets in LiFeAs imply a large density of states near the Fermi surface, which should promote ferromagnetic (FM), instead of the usual AF, spin fluctuations for superconductivity.[19] If this is indeed the case, AF spin fluctuations should not be fundamental to the superconductivity of FeAs-based materials and the superconducting pairing would not be in the spin singlet channel. A determination of the magnetic properties in LiFeAs is thus important to complete our understanding about the role of magnetism in the superconductivity of FeAs-based materials.

In this paper, we present inelastic neutron scattering measurements on single crystals of nonsuperconducting $Li_{1-x}FeAs$ with $x = 0.06 \pm 0.01$, where there is no static AF order. As a function of increasing energy, spin excitations in $Li_{0.94}FeAs$ have a spin gap below $\Delta \approx 13$ meV, are centered at the AF wave vector $Q = (1,0)$ for energies up to $\sim$80 meV, and then split into two vertical bands of scattering before moving to the zone boundaries at the wave vectors $Q' = (\pm 1/2, \pm 1/2)$ near $E \approx 130$ meV. These Q' vectors have been observed in the spin excitations of FeTe/Se compounds and imply the existence of a strong competition between FM and AF exchange couplings.[20] While the dispersions of the low-energy spin excitations ($E \leqslant 80$ meV) in $Li_{0.94}FeAs$ are similar to that of $(Ba,Ca,Sr)Fe_2As_2$,[21–23] the high-energy spin excitations near the zone boundary are quite different from these materials, and cannot be modeled from a simple Heisenberg Hamiltonian with effective nearest (J_{1a} and J_{1b}) and next nearest neighbor (J_2) exchange couplings.[21,22] By integrating the local susceptibility $\chi''(\omega)$ in absolute units over the entire bandwidth of spin excitations, we find the spin fluctuating moment $\langle m^2 \rangle = 2.1 \pm 0.6\ \mu_B^2$, a value that is comparable with other pnictides. Therefore, spin excitations in $Li_{0.94}FeAs$ are similar to other iron pnictides but are not directly associated with Fermi surface nesting from hole and electron pockets, contrary to expectations from local density approximation calculations.[18,19]

Our experiments were carried out on the ARCS time-of-flight chopper spectrometer at the Spallation Neutron Source, Oak Ridge National Laboratory. We also performed thermal triple-axis spectrometer measurements on the BT-7 triple-axis spectrometer at NIST Center for Neutron Research. Our single crystals were grown using the flux method and inductively coupled plasma analysis on the samples showed that the compositions of the crystals are $Li_{0.94\pm0.01}FeAs$. Figure 1(b) shows zero-field-cooled (ZFC) and field-cooled (FC) susceptibility measurements on $Li_{0.94}FeAs$, which

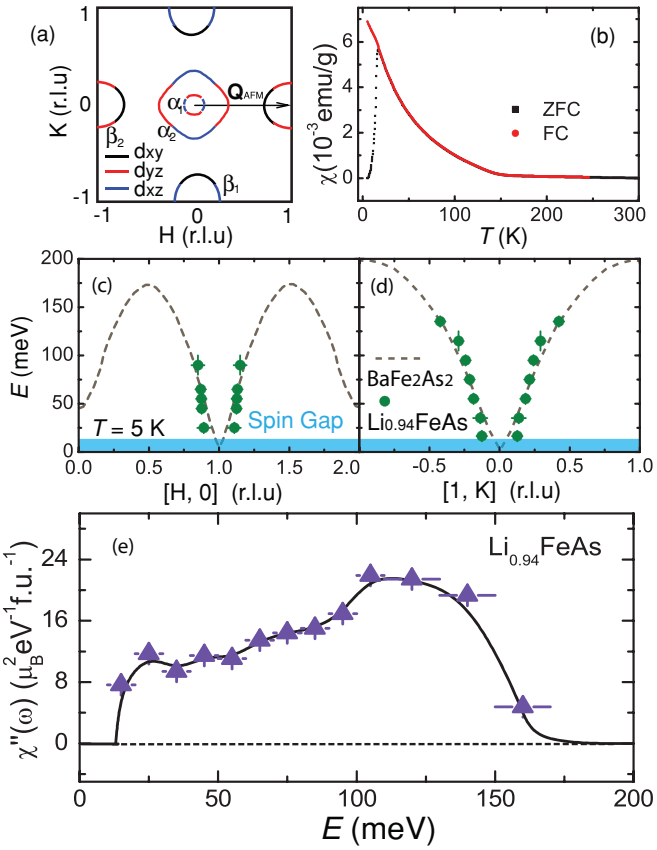

FIG. 1. (Color online) (a) Fermi surfaces from the spin-restricted local density approximation calculation for LiFeAs.[18,19] There are two hole-like Fermi surfaces near the $\Gamma(0,0)$ point with d_{yz}/d_{xz} character and one electron-like Fermi surface near the $M(1,0)$ point. The nesting condition for the expected AF nesting wave vector $Q_{\rm AFM} = (1,0)$ is not favorable.[18] (b) Zero-field-cooled (ZFC) and field-cooled (FC) susceptibility measurements on $Li_{0.94}FeAs$. No superconductivity was observed due to Li deficiency. (c,d) The dashed lines show spin wave dispersions along the $[H,0]$ and $[1,K]$ directions for $BaFe_2As_2$ at 5 K.[21] The filled circles show the measured spin excitation dispersions along the $[H,0]$ and $[1,K]$ directions for $Li_{0.94}FeAs$. While spin waves in $BaFe_2As_2$ extend up to 200 meV along the $[1,K]$ direction, spin excitations in $Li_{0.94}FeAs$ reach the zone boundary near $Q = (1,0.5)$. (e) The energy dependence of the local susceptibility. The solid line is a guide to the eye.

indicate spin glass behavior with no evidence for superconductivity. To study the spin excitations, we co-aligned 7.5 g of single crystals of $Li_{0.94}FeAs$ (with a mosaic of 2°) and loaded the samples inside a He refrigerator or cryostat. To facilitate easy comparison with spin wave measurements in $BaFe_2As_2$,[21] we define the wave vector Q at (q_x, q_y, q_z) as $(H,K,L) = (q_x a/2\pi, q_y b/2\pi, q_z c/2\pi)$ reciprocal lattice units (rlu), where $a = b = 5.316$ Å, and $c = 6.306$ Å. For both triple-axis and ARCS measurements, we aligned crystals in the $[H,0,L]$ scattering zone. The ARCS data are normalized to absolute units using a vanadium standard. The incident beam energies were $E_i = 80, 140, 250$ meV with E_i parallel to the c axis.

Before describing in detail the spin excitation dispersion curves and dynamic local susceptibility in Figs. 1(c)–1(e), we first discuss the triple-axis measurements on the static AF

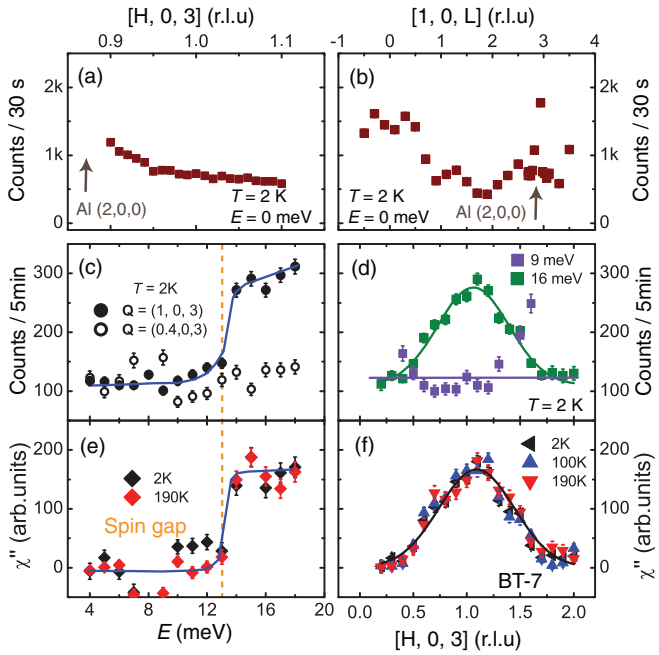

FIG. 2. (Color online) Triple-axis measurements to search for static AF order and spin excitations in $Li_{0.94}FeAs$. (a) Elastic scattering along the $[H,0,3]$ and (b) $[1,0,L]$ directions at 2 K show no evidence of AF order at the expected position $Q = (1,0,3)$. The arrows indicate Al sample holder scattering. (c) Constant-Q scans at the wave vectors $Q = (1,0,3)$ (signal) and $Q = (0.4,0,3)$ (background) positions at 2 K. A clear spin gap is seen at $\Delta = 13$meV. (d) Constant-energy scans at $E = 9$, 16 meV along the $[H,0,3]$ direction. While the scan at $E = 9$ meV is featureless, a clear peak is seen at $E = 16$ meV confirming the spin gap. (e) Imaginary part of the dynamic susceptibility χ'' at 2 K and 190 K. The magnitude of the spin gap is unchanged between 2 and 190 K. (f) Temperature dependence of $\chi''(Q)$ at $E = 16$ meV for 2, 100, and 190 K. $\chi''(Q)$ is almost temperature independent between 2 K and 190 K. Error bars where indicated represent one standard deviation.

order and spin excitations. Figures 2(a) and 2(b) show elastic scattering along the $[H,0,3]$ and $[1,0,L]$ directions across the expected AF peak position (1,0,3), respectively. In contrast to $Na_{1-x}FeAs$, where static AF order is clearly observed,[24] there is no evidence for static AF order in this sample. To search for AF spin excitations, we carried out constant-Q scans at the AF wave vector $Q = (1,0,3)$ and background (0.4,0,3) positions. The outcome in Fig. 2(c) shows a step-like increase in scattering above background for $E > 13$ meV, clearly suggesting the presence of a large spin gap of $\Delta = 13$ meV. To confirm there is indeed a spin gap, we carried out constant-energy scans along the $[H,0,3]$ direction at $E = 9$ and 16 meV as shown in Fig. 2(d). While the scattering is featureless at $E = 9$ meV, there is a clear peak centered at $Q = (1,0,3)$ at $E = 16$ meV. Figure 2(e) shows the temperature dependence of the imaginary part of the dynamic susceptibility $\chi''(E)$ obtained by subtracting the background and correcting for the Bose population factor. Surprisingly, the spin gap has no observable temperature dependence between 2 K and 190 K, much different from the temperature dependence of the spin gaps in the (Ba,Sr,Ca)Fe_2As_2 family of materials,[25–27] which disappear rapidly with increasing temperature. The weak temperature dependence of the dynamic susceptibility has

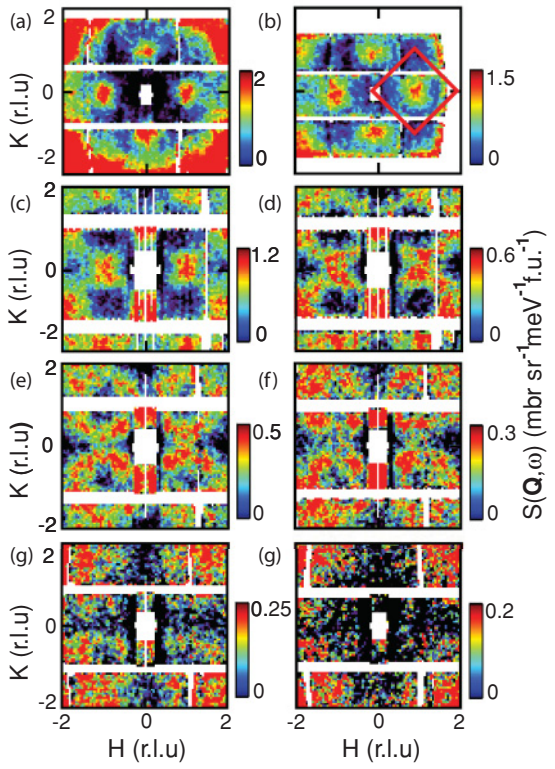

FIG. 3. (Color online) Constant-energy images of the scattering in the $[H,K]$ zone as a function of increasing energy for $Li_{0.94}FeAs$ at energy transfers of (a) $E = 25 \pm 5$ meV; (b) 45 ± 5 meV (with $E_i = 80$ meV); (c) 70 ± 10 meV; (d) 90 ± 10 meV; (e) 110 ± 10 meV; (f) 130 ± 10 meV; (g) 150 ± 10 meV; (h) 170 ± 10 meV, all with $E_i = 250$ meV. The scattering intensity is in absolute units. The box in (b) shows the Brillouin zone used to integrate the susceptibility.

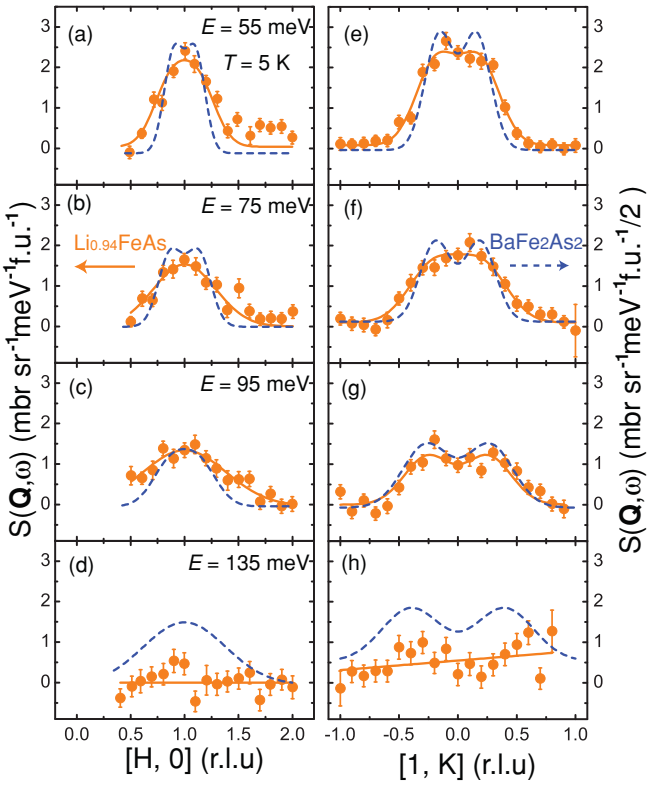

FIG. 4. (Color online) Constant-energy cuts of the spin excitation dispersion as a function of increasing energy along the $[H,0]$ and $[1,K]$ directions for $Li_{0.94}FeAs$. The dashed curves show identical cuts for spin waves of $BaFe_2As_2$ normalized per Fe.[21] Both are in absolute units. Constant-energy cuts along the $[H,0]$ direction at (a) 55 ± 5, (b) 75 ± 5, (c) 95 ± 10, and (d) 135 ± 10 meV. Similar cuts along the $[1,K,]$ direction are shown in (e)–(h). The dynamic spin correlation length is $\xi \approx 12 \pm 3$ Å.

been confirmed by constant-energy scans in Fig. 2(f), where $\chi''(Q)$ at $E = 16$ meV remains essentially unchanged from 2 K to 190 K.

Figure 3 summarizes the ARCS time-of-flight measurements on $Li_{0.94}FeAs$ at 5 K. Since spin excitations in $Li_{0.94}FeAs$ have no c-axis modulations, we show in Figs. 3(a)–3(h) two-dimensional constant-energy (E) images of the scattering in the (H,K) plane for $E = 25 \pm 5$, 45 ± 5, 70 ± 10, 90 ± 10, 110 ± 10, 130 ± 10, 150 ± 10, and 170 ± 10 meV, respectively. For energies between $25 \pm 5 \leqslant E \leqslant 90 \pm 10$ meV, spin excitations form transversely elongated ellipses centered around AF $Q = (1,0)$. The intensity of spin excitations which decreases with increasing energy, which is remarkably similar to spin waves in $BaFe_2As_2$.[21] For energies above 90 meV, spin excitations split into two horizontal arcs that separate further with increasing energy. The excitations finally merge into $Q = (m \pm 0.5, n \pm 0.5)$ $(m,n = 0,1,2)$ and become weaker above 150 meV in Figs. 3(g) and 3(h).

In order to determine the dispersion of spin excitations for $Li_{0.94}FeAs$, we show in Fig. 4 cuts through the two-dimensional images in Fig. 3 and compare with identical cuts for $BaFe_2As_2$. Figures 4(a)–4(d) show constant-energy cuts along the $[H,0]$ direction for energies of $E = 55 \pm 5$, 75 ± 5, 95 ± 5, 135 ± 5 meV, respectively, while the dashed lines show identical spin wave cuts for $BaFe_2As_2$.[21] Since both measurements were taken in absolute units, we can see that spin excitations in $Li_{0.94}FeAs$ are similar to that of $BaFe_2As_2$ per Fe below 95 meV.[21] Figures 4(e)–4(h) show constant-energy cuts along the $[1,K]$ direction for identical energies as that of Figs. 4(a)–4(d). For energies above 95 meV, the strength of the spin excitations in $Li_{0.94}FeAs$ is rapidly suppressed compared to that of $BaFe_2As_2$ and become very weak above $E = 135$ meV. This can originate from an absence of magnetic scattering, or that the scattering is very broad as might occur for an itinerant electron system interacting with Stoner excitations. This is different from spin waves in $BaFe_2As_2$, which extend up to 250 meV. Based on these constant-energy cuts, we show in Figs. 1(c) and 1(d) the comparison of spin excitation dispersions of $Li_{0.94}FeAs$ (filled circles) with those of spin waves in $BaFe_2As_2$ (dashed lines). They are similar for energies between 50–95 meV, while the spin excitations in $Li_{0.94}FeAs$ are broader below 50 meV.

We have attempted, but failed, to use a simple Heisenberg Hamiltonian with effective nearest and next nearest neighbor exchange couplings to fit the observed spin excitation spectra.[21,22] For all possible combinations of the J_{1a}, J_{1b}, and J_2, the expected zone boundary spin excitations are quite different from the observed spectra (see EPAPS information).[28] If we include the next-next-nearest-neighbor exchange coupling

J_3, the expected spectra near the zone boundary have some resemblance to the data in Fig. 3 although the low-energy excitations would be different.[28] This means that the effective exchange couplings in $Li_{0.94}FeAs$ are extremely long-ranged, a hallmark that itinerant electrons are important for spin excitations in this material. Since the data close to the band top along the $[1,K]$ direction are higher in energy than along the $[H,0]$ direction, we need $J_{1b} < 0$ to recover this feature in a J_{1a}-J_{1b}-J_2-J_3 model. This means that effective exchange interactions in $Li_{0.94}FeAs$ may be similar to the (Ca,Sr,Ba)Fe_2As_2 iron pnictides[21–23] in spite of their different zone boundary spectra.

Finally, we show in Fig. 1(e) the energy dependence of the local susceptibility, defined as $\chi''(E) = \int \chi''(\mathbf{q},E)d\mathbf{q}/\int d\mathbf{q}$, where the average is over the magnetic scattering signal $\chi''(\mathbf{q},E)$ over the Brillouin zone [Fig. 3(b)].[29] The corresponding fluctuating moment $\langle m^2\rangle = 2.1 \pm 0.6\ \mu_B^2$ per formula unit. We can use both pure local and itinerant spin models to sketch a basic physical picture based on the moment value. If we assume a quantum local spin model to describe the fluctuations, the moment value implies the spin value is about one. If we take a pure itinerant model, our result would suggest that at least three electrons per iron site occupy the states with energies up to the magnetic bandwidth (∼150 meV) below the Fermi energy. This suggests that the bandwidths of the electron bands near the Fermi surface are narrow. In other words, the band renormalization factors are large and the electron-electron correlations must be strong.

In summary, we measured spin excitations in single crystals of $Li_{0.94}FeAs$. Similar to other iron pnictides, the low energy excitations are still strongly AF.[30] However, comparing to other iron pnictides, they have several distinct properties: (a) a larger spin gap, close to 13 meV that is essentially temperature independent below 190 K; (b) a comparable total magnetic bandwidth; (c) different wave vectors at the zone boundary for high energy excitations. Moreover, the excitations can not be described by magnetic models with only short range magnetic exchange couplings. Our results suggest the AF spin fluctuations are fundamental to the superconductivity of FeAs-based materials. FM fluctuations exist in $Li_{0.94}FeAs$, but they only affect the high energy spin excitations.

We have become aware of a related work on powder samples of superconducting LiFeAs, where AF spin fluctuations have been reported.[31]

The work in IOP is supported by CAS, the MOST of China, and NSFC. This work is also supported by the US DOE BES No. DE-FG02-05ER46202, and by the US DOE, Division of Scientific User Facilities.

*pdai@utk.edu

[1] D. C. Johnston, Adv. Phys. **59**, 803 (2010).
[2] M. D. Lumsden and A. D. Christianson, J. Phys. Condens. Matter **22**, 203203 (2010).
[3] J. W. Lynn and P. C. Dai, Physica C **469**, 469 (2009).
[4] Y. Kamihara *et al.*, J. Am. Chem. Soc. **130**, 3296 (2008).
[5] I. I. Mazin, D. J. Singh, M. D. Johannes, and M. H. Du, Phys. Rev. Lett. **101**, 057003 (2008).
[6] J. Dong *et al.*, Europhys. Lett. **83**, 27006 (2008).
[7] C. de la Cruz *et al.*, Nature (London) **453**, 899 (2008).
[8] H. Ding *et al.*, Europhys. Lett. **83**, 47001 (2008).
[9] K. Seo, B. A. Bernevig, and J. Hu, Phys. Rev. Lett. **101**, 206404 (2008).
[10] K. Kuroki, S. Onari, R. Arita, H. Usui, Y. Tanaka, H. Kontani, and H. Aoki, Phys. Rev. Lett. **101**, 087004 (2008).
[11] A. V. Chubukov, Physica C **469**, 640 (2009).
[12] F. Wang, H. Zhai, Y. Ran, A. Vishwanath, and D. H. Lee, Phys. Rev. Lett. **102**, 047005 (2009).
[13] X. C. Wang *et al.*, Solid State Commun. **148**, 538 (2008).
[14] J. H. Tapp, Z. Tang, B. Lv, K. Sasmal, B. Lorenz, P. C. W. Chu, and A. M. Guloy, Phys. Rev. B **78**, 060505(R) (2008).
[15] M. J. Pitcher *et al.*, Chem. Commun. 5918 (2008).
[16] F. L. Pratt, P. J. Baker, S. J. Blundell, T. Lancaster, H. J. Lewtas, P. Adamson, M. J. Pitcher, D. R. Parker, and S. J. Clarke, Phys. Rev. B **79**, 052508 (2009).
[17] C. W. Chu *et al.*, Physica C **469**, 326 (2009).
[18] S. V. Borisenko *et al.*, Phys. Rev. Lett. **105**, 067002 (2010).
[19] P. M. R. Brydon, M. Daghofer, C. Timm, and J. vandenBrink, Phys. Rev. B **83**, 060501(R) (2011).
[20] O. J. Lipscombe, G. F. Chen, C. Fang, T. G. Perring, D. L. Abernathy, A. D. Christianson, T. Egami, N. Wang, J. Hu, and P. Dai, Phys. Rev. Lett. **106**, 057004 (2011).
[21] L. W. Harriger *et al.*, e-print arXiv:1011.3771.
[22] J. Zhao *et al.*, Nat. Phys. **5**, 555 (2009).
[23] R. A. Ewings *et al.*, e-print arXiv:1011.3831.
[24] S. L. Li, C. delaCruz, Q. Huang, G. F. Chen, T. L. Xia, J. L. Luo, N. L. Wang, and P. Dai, Phys. Rev. B **80**, 020504(R) (2009).
[25] K. Matan, R. Morinaga, K. Iida, and T. J. Sato, Phys. Rev. B **79**, 054526 (2009).
[26] J. Zhao *et al.*, Phys. Rev. Lett. **101**, 167203 (2008).
[27] R. J. McQueeney *et al.*, Phys. Rev. Lett. **101**, 227205 (2008).
[28] See supplemental material at [http://link.aps.org/supplemental/10.1103/PhysRevB.83.220515] for details of the analysis.
[29] C. Lester, J. H. Chu, J. G. Analytis, T. G. Perring, I. R. Fisher, and S. M. Hayden, Phys. Rev. B **81**, 064505 (2010).
[30] C. Platt, R. Thomale, and W. Hanke, e-print arXiv:1103.2101v1.
[31] A. E. Taylor *et al.*, Phys. Rev. B **83**, 220514 (2011).

Supplementary Information: Antiferromagnetic spin excitations in single crystals of nonsuperconducting $Li_{0.94}FeAs$

Meng Wang, X. C. Wang, D. L. Abernathy, L. W. Harriger, H. Q. Luo, Yang Zhao, J. W. Lynn, Q. Q. Liu, C. Q. Jin, Chen Fang, Jiangping Hu, and Pengcheng Dai

PACS numbers:

In order to test if a simple J_{1a}-J_{1b}-J_2-J_3 Heisenberg Hamiltonian can reproduce the observed spin excitations spectra in Fig. 3, we simulated the expected spin wave spectra using Heisenberg Hamiltonian [1]. To facilitate direct comparison with the data in Fig. 3, we normalized the calculated intesity at 90 meV to be the same as that in Fig. 3. Therefore, the calculated spectra can be directly compared with the observed spectra. Figure SI1 shows spin wave calculations assuming $SJ_{1a} = 23$ meV, $SJ_{1b} = -4$ meV, $SJ_2 = 13$ meV, and $SJ_3 = -5$ meV. While the zone boundary spectra have some similarity to the data, the spectra clearly disagree with the data around intermediate energies. Figure SI2 shows similar calculation assuming $SJ_{1a} = SJ_{1b} = 10$ meV, $SJ_2 = 20$ meV, and $SJ_3 = -8$ meV. Figure SI3 plots calculations assuming $SJ_{1a} = 23$ meV, $SJ_{1b} = -4$ meV, $SJ_2 = 13$ meV, and $SJ_3 = 0$ meV; and Figure SI4 show calculation with $SJ_{1a} = SJ_{1b} = 10$ meV, $SJ_2 = 20$ meV, and $SJ_3 = 0$ meV. The spin wave band tops are in Figs. SI1-SI4 are 150 meV, 150 meV, 110 meV, and 100 meV, respectively. To obtain similar scattering pattern as observed near the band top by a Heisenberg Hamiltonian with effective exchange couplings, the next-next nearest neighbor exchange coupling J_3 has to be included.

We note that spin excitations close to the band top in Fig1(e) clearly shows that zone boundary energy in the $[1, K]$ direction is higher in energy than that along the $[H, 0]$ direction. In the following we show that in a J_{1a}-J_{1b}-J_2-J_3 model with antiferromagnetic J_{1a} and J_2 and ferromagnetic J_3, we need and only need $J_{1b} < 0$ (ferromagnetic) to recover this feature.

The J_{1a}-J_{1b}-J_2-J_3 model is analogous to the J_{1a}-J_{1b}-J_2 spin model used to describe $CaFe_2As_2$[1]. In the following we will consider a detwinned system, and one should bear in mind that one q-point (q_x, q_y) in a twinned system corresponds to (q_x, q_y) and (q_y, q_x) in a detwinned one. The spinwave dispersion for this model is given by

$$\omega(h,k) = S\sqrt{A^2(h,k) - B^2(h,k)}, \tag{1}$$

where

$$\begin{aligned} A(h,k) &= 2[J_{1b}(\cos(\pi k) - 1) + J_{1a} + 2J_1 + J_3(\cos(2\pi h) + \cos(2\pi k) - 2)], \\ B(h,k) &= 2(J_{1a}\cos(\pi h) + 2J_2\cos(\pi h)\cos(\pi k)). \end{aligned} \tag{2}$$

In the model, the dispersion along $[H, 0]$-direction sees the maximum at $(1/2, 0)$, while along $[1, K]$-direction, the maximum is at $(1, q)$ where $q \sim 1/2$ is in fact parameter dependent. But one should not only compare $\omega(1/2, 0)$ and $\omega(q, 0)$ to find which direction reaches a higher top, because there is twinning. Once we have twinning into play, we also need to compare the band near $(0, 1)$. Mark that in discussing this region, H and K directions should be interchanged when compared with the experimental frame. Starting from $(0, 1)$, the dispersion reaches maximum along K-direction at $(0, 1/2)$ and along H direction at $(1/2, 1)$. Therefore, in order to see what we see in the experiment, we should have

$$\max[\omega(1/2, 0), \omega(0, 1/2)] < \max[\omega(1, q), \omega(1/2, 1)]. \tag{3}$$

Now we make a statement and prove it: $J_{1b} < 0$ is sufficient and necessary for the Eq.(3) to hold. First we prove the sufficiency.

$$\omega^2(1/2, 1) - \omega^2(1/2, 0) = 16J_{1b}(-J_{1a} + J_{1b} - 2J_2 + 2J_3). \tag{4}$$

From this we know if $J_{1b} < 0$, we have $\omega(1/2, 1) > \omega(1/2, 0)$. On the other hand,

$$\omega^2(1/2, 1) - \omega^2(0, 1/2) = 4(J_{1a}^2 - 2J_{1a}J_{1b} + J_{1b}(3J_{1b} - 4J_2 + 4J_3)). \tag{5}$$

From this we know if

$$J_{1b} < \frac{1}{3}(J_{1a} + 2J_2 - 2J_3 - \sqrt{(J_{1a} + 2J_2 - 2J_3)^2 - 3J_{1a}^2}, \tag{6}$$

$\omega(1/2, 1) > \omega(0, 1/2)$.
But of course

$$\frac{1}{3}(J_{1a} + 2J_2 - 2J_3 - \sqrt{(J_{1a} + 2J_2 - 2J_3)^2 - 3J_{1a}^2} > 0, \tag{7}$$

therefore $J_{1b} < 0$ is sufficient to make the highest energy along $[1, K]$ direction higher than $[H, 0]$ direction.

Then we prove the necessity. It is a proof by contradiction. Suppose $J_{1b} > 0$, then from above we know that $\omega(1/2, 1) \leq \omega(1/2, 0)$. Also notice that when $J_{1b} > 0$,

$$\begin{aligned} \omega^2(1, q_y) &= 4(J_{1a} + 2J_2 + J_{1b}(\cos(\pi q) - 1) - 2J_3 \sin^2(\pi q))^2 - 4(J_{1a} + 2J_2 \cos(\pi q))^2 \\ &< 4(J_{1a} + 2J_2 - 2J_3)^2 - 4(J_{1a} - 2J_2)^2 \\ &= 16(J_{1a} - J_3)(2J_2 - J_3) \\ &\leq 4(J_{1a} + 2J_2 - 2J_3)^2 \\ &= \omega^2(1/2, 0). \end{aligned} \tag{8}$$

Therefore

$$\max[\omega(1/2, 0), \omega(0, 1/2)] \geq \max[\omega(1, q), \omega(1/2, 1)]. \tag{9}$$

Therefore we have proved if $J_{1b} > 0$ then the highest energy along $[1, K]$ direction is lower than the highest energy along $[H, 0]$ direction, i.e., $J_{1b} < 0$ is necessary to recover the feature observed in experimental data.

[1] J. Zhao *et al.*, Nat. Phys. **5**, 555 (2009).

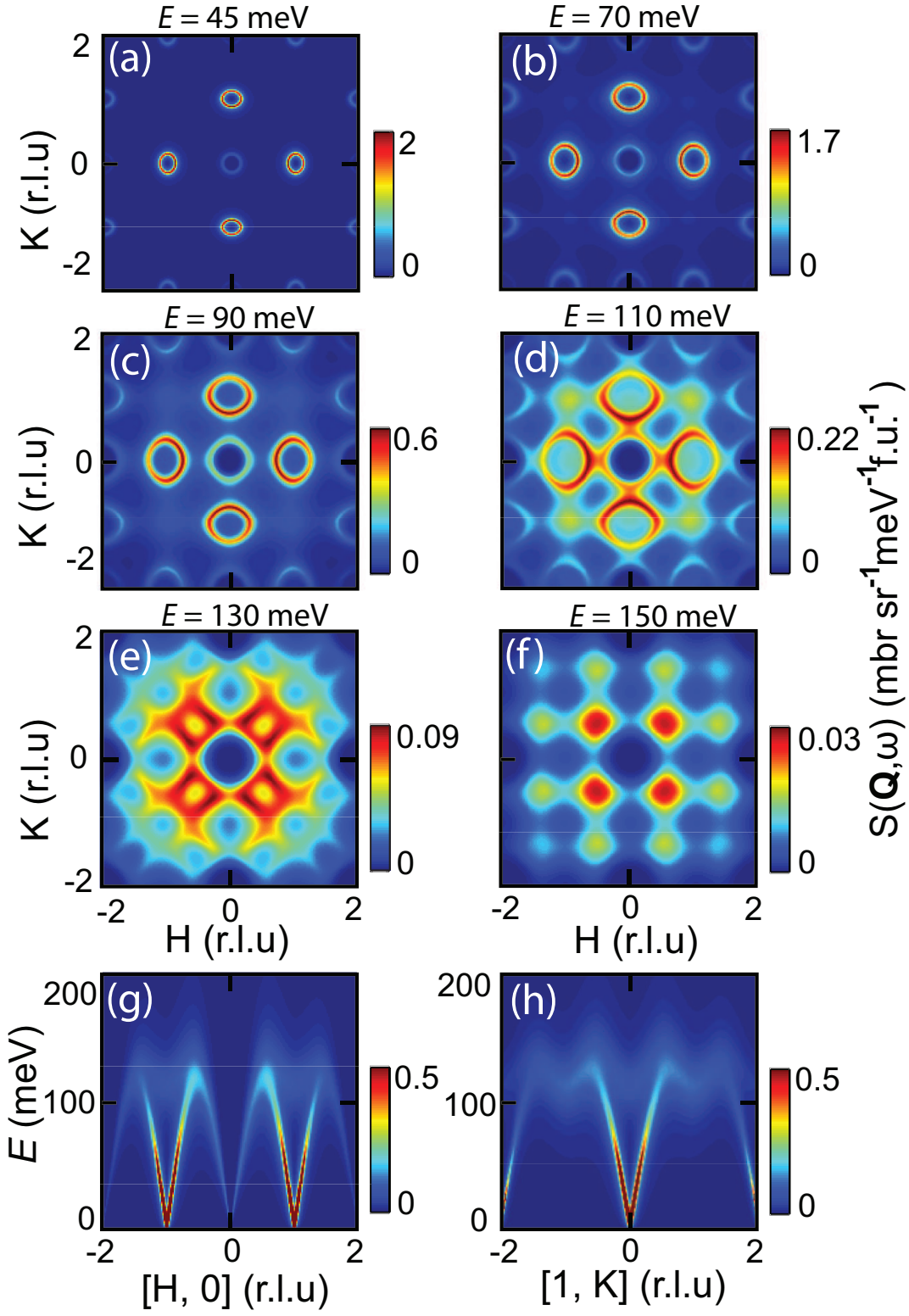

FIG. 1: (color online). Constant-energy images of the scattering in the $[H, K]$ zone as a function of increasing energy for $Li_{0.94}FeAs$ at energy transfers of (a) 45 meV; (b) 70 meV; (c) 90 mV; (d) 110 meV; (e) 130 meV; (f) 150 meV; (g,h) The expected spin wave dispersion along the $[H, 0]$ and $[1, K]$ directions for LiFeAs. The exchange couplings used to obtain these imagines are $SJ_{1a} = 23$ meV, $SJ_{1b} = -4$ meV, $SJ_2 = 13$ meV, $SJ_3 = -5$ meV, and anisotropy factor $SJ_s = 0.08$ meV. Spin wave damping is assumed to be $\Gamma = 0.15E$ throughout the supplementary information.

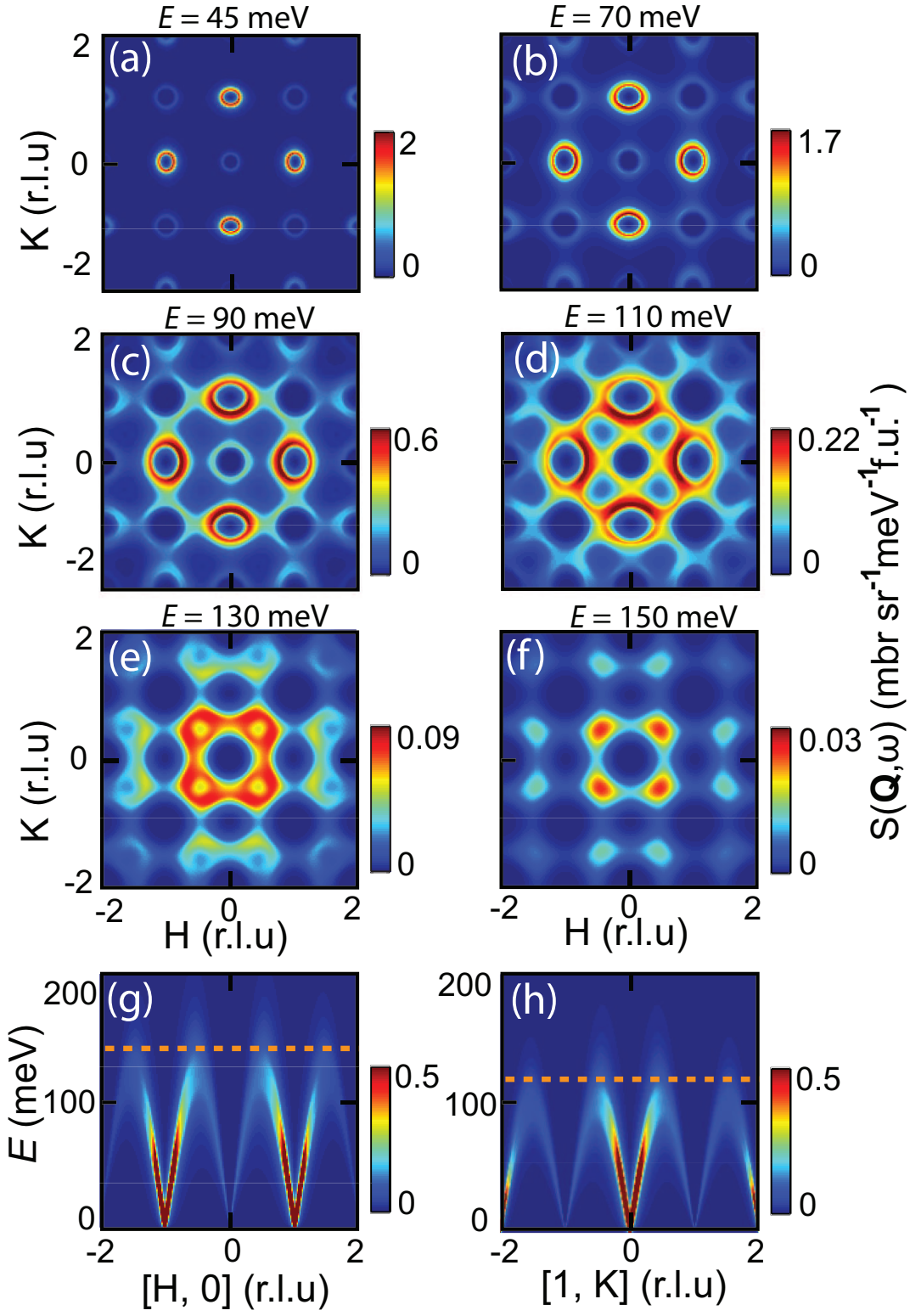

FIG. 2: (color online). Constant-energy images of the scattering in the $[H, K]$ zone as a function of increasing energy for $Li_{0.94}FeAs$ at energy transfers of (a) 45 meV; (b) 70 meV; (c) 90 mV; (d) 110 meV; (e) 130 meV; (f) 150 meV; (g,h) The expected spin wave dispersion along the $[H, 0]$ and $[1, K]$ directions for LiFeAs. The exchange couplings used to obtain these imagines are $SJ_{1a} = 10$ meV, $SJ_{1b} = 10$ meV, $SJ_2 = 20$ meV, $SJ_3 = -8$ meV, and anisotropy factor $SJ_s = 0.08$ meV.

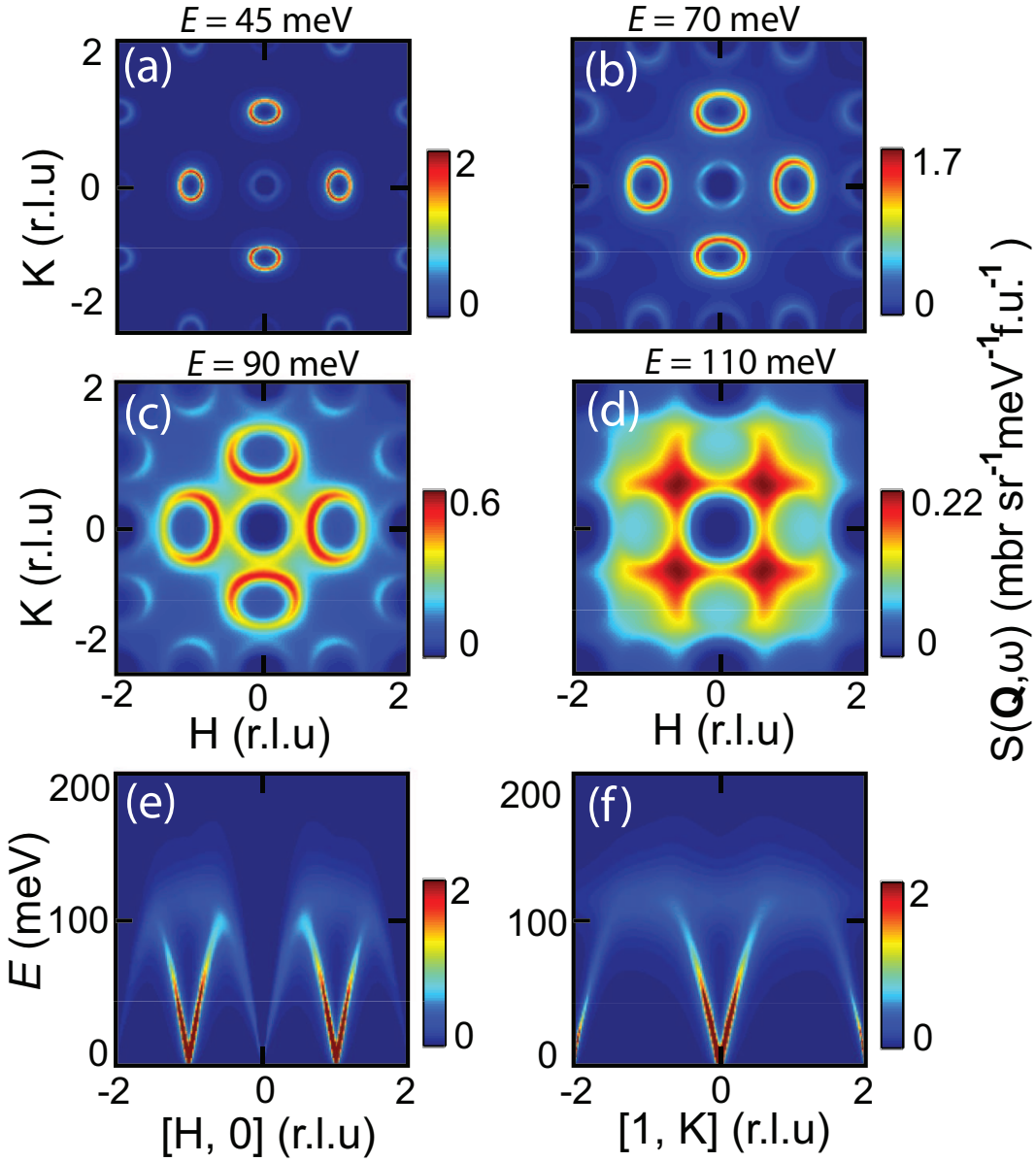

FIG. 3: (color online). Constant-energy images of the scattering in the $[H, K]$ zone as a function of increasing energy for $Li_{0.94}FeAs$ at energy transfers of (a) 45 meV; (b) 70 meV; (c) 90 mV; (d) 110 meV; (e,f) The expected spin wave dispersion along the $[H, 0]$ and $[1, K]$ directions for LiFeAs. The exchange couplings used to obtain these imagines are $SJ_{1a} = 23$ meV, $SJ_{1b} = -4$ meV, $SJ_2 = 13$ meV, $SJ_3 = 0$ meV, and anisotropy factor $SJ_s = 0.08$ meV.

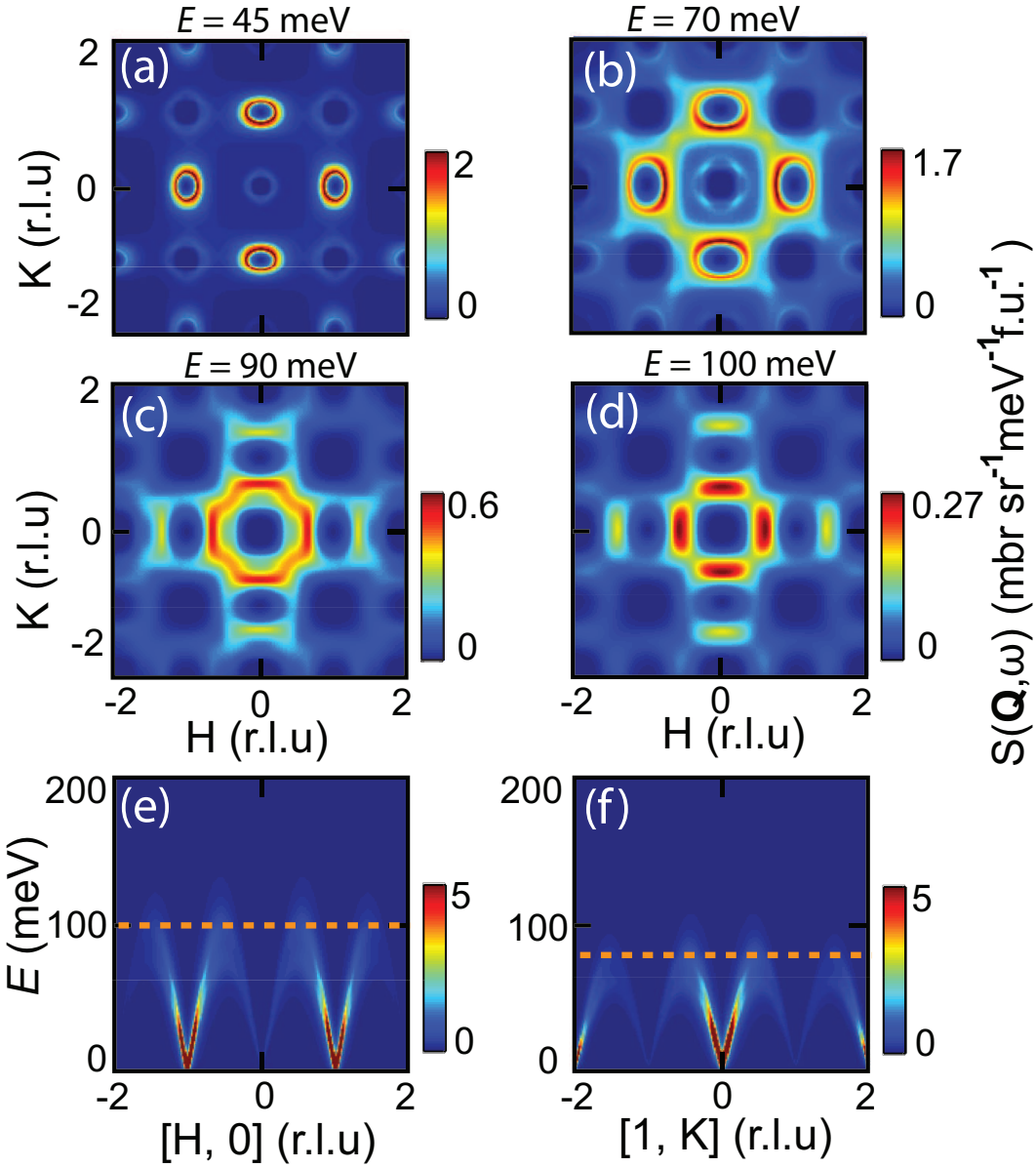

FIG. 4: (color online). Constant-energy images of the scattering in the $[H, K]$ zone as a function of increasing energy for $Li_{0.94}FeAs$ at energy transfers of (a) 45 meV; (b) 70 meV; (c) 90 mV; (d) 100 meV; (e,f) The expected spin wave dispersion along the $[H, 0]$ and $[1, K]$ directions for LiFeAs. The exchange couplings used to obtain these imagines are $SJ_{1a} = 10$ meV, $SJ_{1b} = 10$ meV, $SJ_2 = 20$ meV, $SJ_3 = 0$ meV, and anisotropy factor $SJ_s = 0.08$ meV.